3DoF simulation model and specific aerodynamic control capabilities for a SpaceX's Starship-like atmospheric reentry vehicle

Thibault Cantou, Nicolas Merlinge, Romain Wuilbercq

3DoF simulation model and specific aerodynamic control capabilities for a SpaceX's Starship-like atmospheric reentry vehicle

Thibault CANTOU, Nicolas MERLINGE**, Romain WUILBERCQ****
**ONERA – DTIS – NGPA*
thibault.cantou@onera.fr
***ONERA – DTIS – CEVA*
nicolas.merlinge@onera.fr
****ONERA – DTIS – CEVA*
romain.wuilbercq@onera.fr

Abstract
In September 2018, a novel design of reusable atmospheric reentry vehicle was proposed: SpaceX's Starship (SXS). Its main difference with comparable vehicles lays in its aerodynamic actuators that allow for stable flight at angles of attack (AoA) up to 90°. In this work, we propose a 3DoF simulation model of this vehicle, and present preliminary reentry simulation results. A study of the center of mass location's implications on longitudinal stability is presented. The modulation of the aerodynamic forces at a given equilibrium AoA allowed by the multiactuator configuration is discussed and demonstrated on a reentry trajectory simulation.

1. Introduction

Since the beginning of the space era, the design of vehicles able to survive atmospheric reentry has been a challenging engineering problem. Reentry at orbital or near-orbital velocity implies very intense heat, aerodynamic pressure, and load factor. These issues are tackled with a combination of careful vehicle design (heat shielding or regenerative cooling, tough structure, etc.), and careful mission planning through reentry trajectory optimization if the vehicle has a maneuvering capability.
The reentry trajectory can be divided in two phases: the exo-atmospheric phase, and the atmospheric phase. The latter is the most constraining one due to aerodynamic and aero-thermal effects at high velocity. During the first phase, the trajectory is controlled by exerting thrusts in various directions to track a desired velocity vector (orientation and norm). During the second phase, vehicles will often exploit angle of attack (AoA) and bank angle (BA) control to manoeuver and track a reference constrained trajectory minimizing heating, load factor, and aerodynamic pressure.
Atmospheric trajectory optimization relies a lot on the aerodynamic capabilities of the considered vehicle. The first generations of reentry vehicles (i.e. reentry capsules) needed to be simple, robust to a great amount of uncertainties, and small enough to fit in the rockets of that era. The geometry allowing to deal with those constraints with the technology available at that time was not in favor of a high lift-to-drag ratio vehicles. They were nevertheless somewhat maneuverable during the atmospheric part of the flight (AoA and BA) thanks to center-of-mass (CoM) location control and/or cold gas thrusters for attitude control.
Later, technological progress and the need for reusability allowed the design of rather safe reentry vehicles with more aerodynamically efficient shapes (i.e. with higher lift-to-drag ratio). The Space Shuttle and the X37-B are great examples of such vehicles. Their actuators (similar to those of an aircraft) allow this category of vehicle to remain stable at high AoA during the atmospheric flight. This then generate lift that can be oriented through BA control and used to shape the trajectory as needed.

The subject of this study, a novel design for a reusable atmospheric reentry vehicle, was proposed in September 2018: Space X's Starship (SXS). It exhibits an innovative configuration of aerodynamic control surfaces granting it unique capabilities. The motivation for this work is to give elements to understand why this configuration is an interesting choice. In the following sections, we will:

- Propose an OpenVSP [1] geometrical model of SpaceX's Starship;
- Introduce the methodology used to generate an aerodynamic database for lift, drag, and pitching moment at hypersonic speeds;
- Analyze the implications of this design on longitudinal aerodynamic stability and its dependency to the location of the center of mass ;
- Discuss the implication of the multi-actuator configuration on aerodynamic forces modulation while holding the vehicle at a fixed angle of attack ;
- Provide some atmospheric reentry simulation results to illustrate the performances of the vehicle.

2. Context

SXS will be the second stage of SpaceX's future heavy rocket. It will be mounted on top of the Super Heavy booster. As it is a reusable second stage, SXS needs propulsion in order to reach the orbit, deorbit itself, and achieve a propulsive landing. But it also needs actuators able to control its attitude during atmospheric reentry. Since this study is focused on the behavior of SXS in the hypersonic regime during its reentry, it does not integrate a propulsive model. Figure 1 below presents the reference axis system and some elements of vocabulary used in this study.

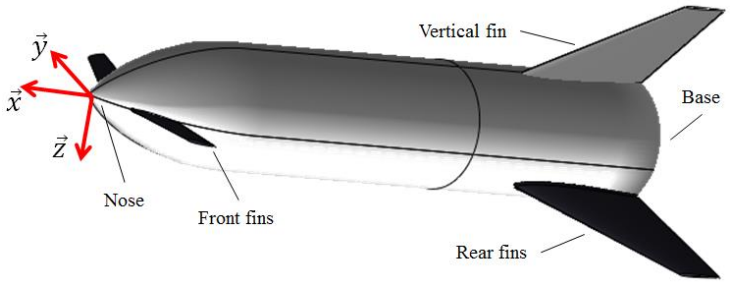

Figure 1 : Body frame and parts of the SXS model

The configuration of SXS's aerodynamic control surfaces is what differentiates it from other reentry vehicles. As showed on the picture below, each actuated fin (colored black) can rotate along an axis tangent to the body at its root chord (the X axis for the rear fins).

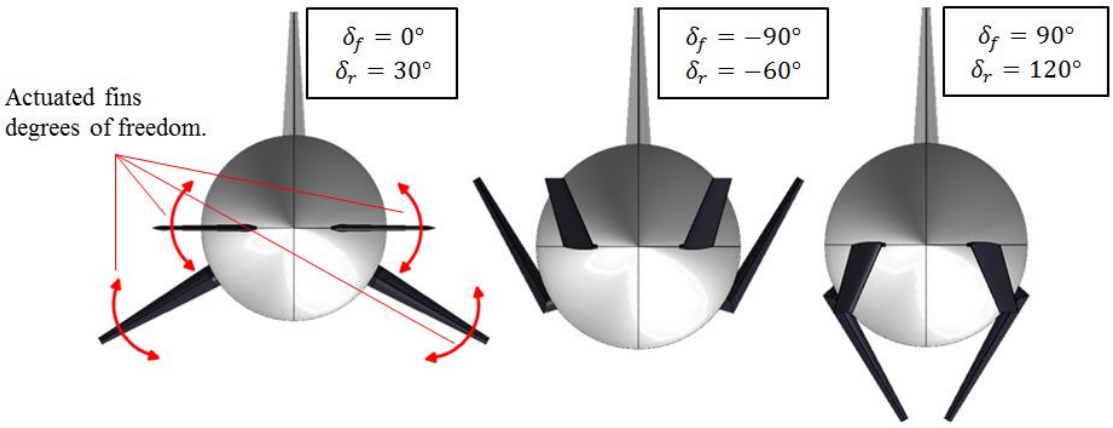

Figure 2 : Degrees of freedom of the actuated fins

The actuated fins will only be used when separated from the booster and in the atmosphere at sufficient speed, i.e. during reentry. As demonstrated in section 4, this aerodynamic control configuration allows the vehicle to achieve aerodynamic stability at AoAs up to 90°, but not for values close to 0° (their rotation axis doesn't allow for torque generation at low AoA). As a matter of comparison, the Space Shuttle was able to control its AoA from 0° to

approximately 40°. This very high AoA stability provides SXS with different manœuvering capabilities that need to be explored.

3. SXS Model creation

3.1. 3D geometry of the vehicle in OpenVSP

The 3D geometry of the vehicle was created in NASA's OpenVSP [1] from photographs. As the vehicle is still in active development, the precise three-dimensional shape varies from a published picture to another. Therefore a representative model of the aerodynamic configuration of SXS has been created rather than a picture perfect model. As stated on SpaceX's website [2], the vehicle's diameter is 9 m, and its length is 55 m including the fins. This allowed us to infer the rest of the required dimensions.

Body:
The body is 51 m long. The ogive section ends at 13 m along the X axis from the nose and then blends into a cylindrical shape until the base of the vehicle.

Actuated fins:
The selected profile is a symmetrical NACA 0010 profile. The planform is modelled the following way:

- Front fins: The front point of the front fins is located 2.6 m rearward the nose on the X axis. At the root, their chord is 3.5 m. At the tip, it is 2.2 m. The section tangent to the body forms an angle of 22° around the Z axis. They span 3 m orthogonally to the first section. The taper ratio is 0.63 and the sweep angle is 30°. The dihedral angle is the control angle and is limited to the range [-90°, 90°].
- Rear fins: The front point of the rear fins is located 37.8 m rearward the nose on the X axis, at an angle of 30° down the XY plane. At the root, their chord is 11.4 m. At the tip, it is 3.7 m. They span 6.2 m orthogonally to the first section. The sweep angle is 64°. The dihedral angle is the control angle and is limited to [-60°, 120°].

Vertical fin:
It is similar to the rear fins but the dihedral angle is kept at -90°.

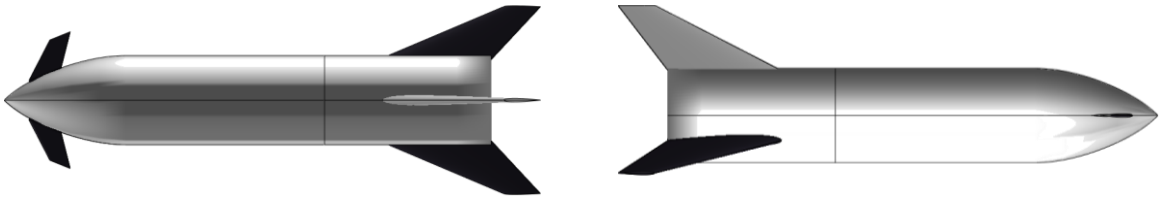

Figure 3 : Up view (left) and right-side view (right) of the OpenVSP model

The convention for the fins control angles is chosen negative up and positive down. To account for the dependency of the aerodynamics to the actuated fins angles, a set of 3D models has been generated for every combination of rear and front fins angles in their respective definition domain with a step angle of 10°. From each of these models, a 3D mesh has been created in OpenVSP and then used in SHAMAN, as described over the next section.

3.2. Reduced-Order Hypersonic Aerodynamics

Future reusable launchers, such as those of interest in the present study, will face some severe aero-thermodynamic loads during their reentry into the terrestrial atmosphere. They will travel from the near-vacuum conditions of space - i.e. in the free-molecular flow regime - to the denser region of the lower atmosphere - i.e. in the continuum flow regime – and through a mixed-density transitional flow regime in between.
In the context of this study however, since the reentry trajectory of the Starship occurs mostly in regions where the flow behaves as a continuum, it is assumed that methods that are valid in this regime can be applied throughout the flight envelop of the vehicle.
An in-house code, dubbed Shaman, is thus used in order to quantify the inviscid aerodynamics of our vehicle when it operates in the realm of the hypersonic flow regime. Shaman embeds a number of simplified methods, the so-called

Local Surface Inclination (LSI) methods [3]. Those only require, as inputs, a triangulation to describe the geometry of the vehicle being modelled (see Figure 4 below), the local inclination angle of all surface panels and the freestream conditions.

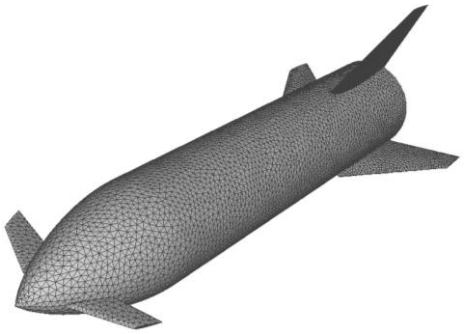

Figure 4 : Unstructured triangular mesh of the Starship (made up of 16800 panels)

The decrease in terms of physical realism that accompanies this panel-based approach, especially when compared to modern numerical methods such as Computation Fluid Dynamics (CFD), is offset almost entirely in many practical applications by its low computational cost and parametric flexibility [4]. Thus, albeit these LSI methods are considered of a low fidelity level, they provide reasonable estimates with regard to the preliminary nature of the analyses presented in this study.
Since the vehicle holds a very high angle-of-attack throughout its reentry trajectory and due to the general bluntness of the Starship, the modified Newtonian theory has been applied to all parts of the configuration geometry.
Assuming a so-called Newtonian flow, the pressure exerted on the vehicle is thus considered solely due to the total loss of momentum of the fluid in the direction normal to the vehicle's surface [3]. The local pressure coefficient $C_{p,i}$ at any panel i is then given by:

$$C_{p,i} = C_{p,max} \sin^2 \theta_i \quad \textbf{(1)}$$

Where θ_i is the local inclination angle between the freestream flow direction and a tangent to the local surface panel.
As suggested by the work of Lester Lees [5], the modified Newtonian theory accounts for the total pressure loss across the normal shock that is located ahead of the vehicle. Therefore, $C_{p,max}$ is equal to the pressure coefficient at the stagnation point behind a normal shock.
A database of aerodynamic coefficients (i.e. C_L, C_D and $C_{m/ref}$) has then been created as a function of the freestream Mach number M_∞ (from Mach 4 to Mach 30), the vehicle's angle-of-attack α (from 0° to 180°), and the front and rear control fins angles (respectively from -90° to 90°, and from -60° to 120°). Some results from the aerodynamic database without any deflection of the control surfaces ($\delta = 0°$) are presented in Figure 5.
The aerodynamic coefficients can then be interpolated in order to provide estimates at any particular point along the trajectory profile through the use of the reference properties associated with our SXS configuration (S_{ref} and L_{ref}) and the dynamic pressure. These reference quantities are provided in Table 1. It shall finally be borne in mind that viscous effects have been neglected in this preliminary work.

Table 1 : Reference Properties for the Aerodynamics of the Starship

Reference	**Value**	**Remark**
Length, L_{ref} [m]	9	Fuselage Diameter
Area, S_{ref} [m^2]	64	Fuselage Circular Cross-Section
Reference Point for Moments [m]	[-25, 0, 0]	The origin is located at the nose of the vehicle

3DoF simulation model and specific aerodynamic control capabilities for a Space X's Starship-like atmospheric reentry vehicle.

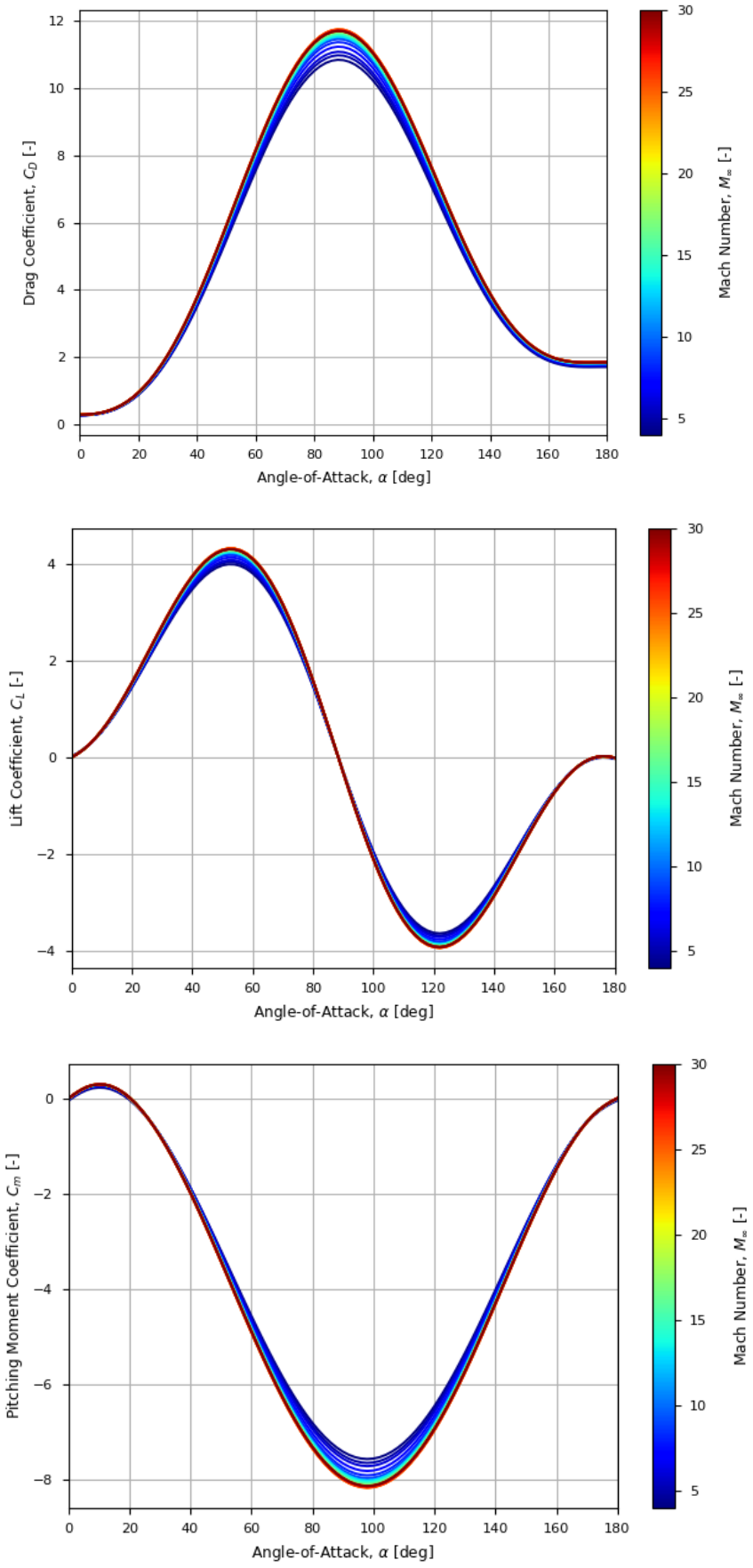

Figure 5 : Aerodynamic Coefficients at $\delta_r = 0°$ and $\delta_f = 0°$

The aerodynamic forces and moment in wind axis are to be computed with the following expressions:

$$F_{Lift} = -Q.S_{ref}.C_L \quad \textbf{(2)}$$

$$F_{Drag} = -Q.S_{ref}.C_D \quad \textbf{(3)}$$

$$M_{Pitch} = Q.S.l.C_{m/ref} \quad \textbf{(4)}$$

In the body axis system, the vector forces' expressions are:

$$\overrightarrow{F_{Axial}} = -Q.S_{ref}.C_A.\vec{x} \quad \textbf{(5)}$$

$$\overrightarrow{F_{Normal}} = -Q.S_{ref}.C_N.\vec{z} \quad \textbf{(6)}$$

With:

$$C_A = C_D.\cos(\alpha) - C_L.\sin(\alpha) \quad \textbf{(7)}$$

$$C_z = C_D.\sin(\alpha) + C_L.\cos(\alpha) \quad \textbf{(8)}$$

3.3. Mass and center of mass

The vehicle's dry mass is estimated to be 85 tons [6]. The simulation results displayed in section 6 are based on this dry mass hypothesis, although this value excludes the fuel needed for the landing burn. A study including a propulsive model would be needed to estimate the required fuel mass needed for this part of the flight and then use a more representative mass during reentry simulation.

As demonstrated in the next section, the location of the center of mass has a great influence on the AoA solution for the pitch moment equation equilibrium. We assume that its coordinates in Y and Z are 0, and will only study the influence of variations of its X coordinate. Since the engines have a significant mass, and that most of the fuel has already been burnt before its reentry, the CoM is likely to be closer to the base than to the nose of the vehicle along the X axis. In the next section, we will study aerodynamic stability depending on the CoM's location. In section 6, the CoM will be considered still in the body frame and located 30 m behind the nose of the vehicle on the X axis.

4. Pitch equilibrium analysis and sensitivity to CoM location

4.1. Coefficient of moment at CoM

In order to study the influence of the CoM's location on the pitch equilibrium of the vehicle, the aerodynamic moment is expressed at the center of mass location ($\wedge$ being the cross-product operator):

$$\overrightarrow{M_{CoM}} = \overrightarrow{M_{CRM}} + \left(\overrightarrow{CRM} - \overrightarrow{CoM}\right) \wedge \overrightarrow{F_{aero}} \quad \textbf{(9)}$$

Given that this model is contained in the XZ plan, in the body frame the previous equation becomes:

$$\overrightarrow{M_{CoM}}\Big|_{body} = Q.S.l.Cm_{CRM}.\vec{y} + \begin{pmatrix} X_{CRM} - X_{CoM} \\ 0 \\ 0 \end{pmatrix} \wedge \begin{pmatrix} -CA \\ 0 \\ -CN \end{pmatrix} \quad \textbf{(10)}$$

With MY_{CoM} being the second component of the total aerodynamic moment in the body frame, we have:

$$MY_{CoM} = Q.S.(l.Cm_{CRM} + (X_{CRM} - X_{CoM}).CN) \quad \textbf{(11)}$$

3DoF simulation model and specific aerodynamic control capabilities for a Space X's Starship-like atmospheric reentry vehicle.

$$MY_{CoM} = Q.S.l.Cm_{CoM} \tag{12}$$

With Cm_{CoM}:

$$Cm_{CoM} = Cm_{CRM} + \frac{X_{CRM} - X_{CoM}}{l}.CN \tag{13}$$

Cm_{CoM} is a function of Mach, AoA, CoM location, δ_r, and δ_f. Solving for the AoA, the zeros of Cm_{CoM} are the equilibrium points of the pitching moment equation. Moreover, an equilibrium point is open-loop locally stable if the slope of Cm_{CoM} is negative. For safety reasons, open-loop rotational stability of the vehicle during atmospheric reentry is a desirable behavior.

4.2. Cm_{CoM} VS Mach

In this paragraph, the CoM is considered located at -27.5 m on the X axis. The following curves show the evolution of Cm_{CoM} against AoA for several Mach values, and for two sets of fins angles : 0° both (fins parallel to the XY plan), and -90° front and -60° rear (maximum fins angle above the XY plan, cf. middle picture of Figure 2):

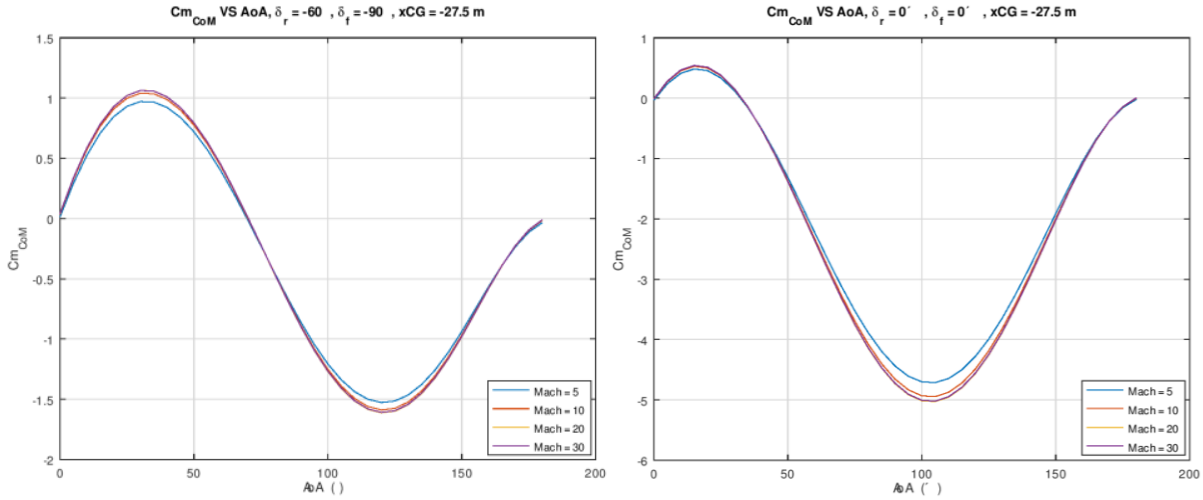

Figure 6 : Variation of Cm_{CoM} versus Mach number for a CoM located at -27.5 m on the X axis

In the left case, each curve crosses 0 with a negative slope between 32,5°+/-0,5°. In the second one, each curve crosses 0 between 70°+/-0,5°. These results show that the Mach number has little effect on the value of equilibrium AoA, but also on the overall values of Cm_{CoM}. This means that the conclusions we can draw at a given point of the flight domain are valid on the whole Mach number domain. However, this is true only for the study of the stabilized/final values of the open-loop. The dynamical characteristics of the open-loop remain very dependent on the Mach number because of the dynamic pressure.

4.3. Cm_{CoM}VS CoM location

In this paragraph, we focus on the sensitivity of the pitching moment to the location of the CoM. In order to reduce the complexity of the analysis, we will only consider the two following extreme configurations of the fins angles (i.e. negative values of the angles):

- The first configuration is when the rear fins are at 0° (maximally exposed to the airflow) and the front fins are at 90° up (minimally exposed to the airflow). This configuration corresponds to the case of lowest equilibrium AoA. The rear fins act like the pitch stabilizers of an airplane's tail (cf. blue curve on Figure 7).

- The second configuration is the opposite: the rear fins are at 60° up (minimally exposed to the airflow) and the front fins are at 0° (maximally exposed to the airflow). This corresponds to the case of highest equilibrium AoA (cf. orange curve on Figure 7).

We deliberately limit the control fins angles to the negative part of their domain. This rather restrictive hypothesis is justified by the fact that high positive values of fins angles (i.e. down) when the vehicle is at high AoA implies a high risk of roll instability, while on the contrary high negative values (i.e. up) favor roll stability.
As stated in paragraph 4.2, we can draw general conclusions with acceptable accuracy from the study of one point of Mach. We then arbitrarily choose Mach 15 in the following results. For the two considered fins angles configurations, the following figures display: the Cm_{CoM} versus AoA for several positions of CoM on the left, and the obtained equilibrium AoA versus the CoM's location on the right.

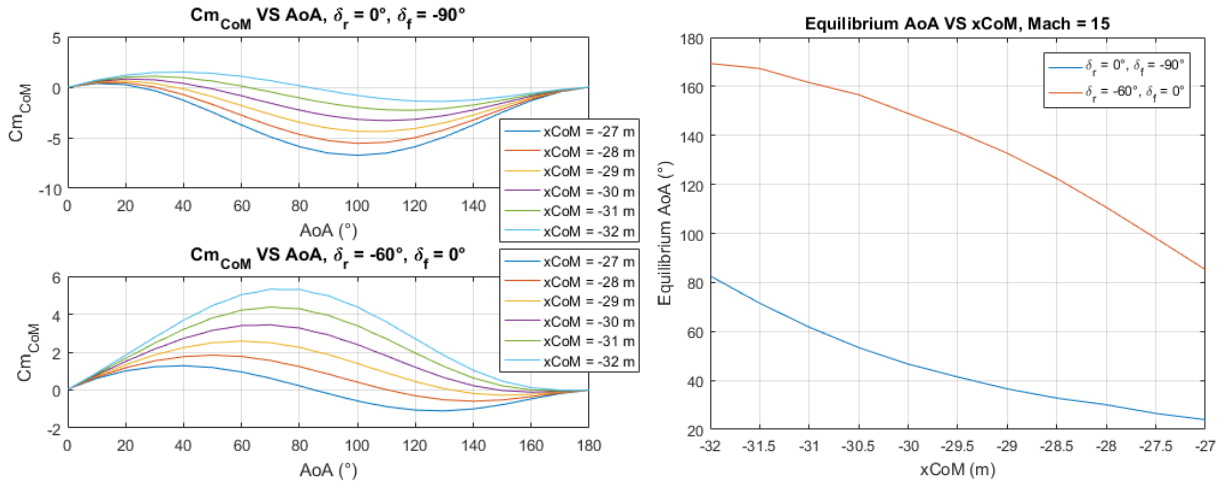

Figure 7 : Variation of Cm_{CoM} versus CoM location along the X axis for the two extreme configurations of fins angles

On the right figure, the distance between the two curves in the Y axis direction is the AoA domain of open-loop stability. What we can observe is that this domain moves towards greater AoAs when the CoM moves back from the nose. For example, if the CoM is 32 m behind the nose, the minimum feasible AoA is about 80°.
At least three requirements will guide the designers in setting a goal for AoA stabilizable domain, which will then influence the selection of the target CoM location:

Propulsion systems protection:
As it is not desirable to frontally expose the nozzles to the hypersonic airflow during reentry, it is necessary for the vehicle's AoA to be in a stable equilibrium between 0° and 90° during the flight. It is also required to minimize the thermal flow. From this standpoint, it is optimal to fly with an AoA comprised between 0° and 90°.

Global heating minimization:
Since the thermal flow highly depends on the curvature of the exposed surface, it reaches a maximum value at 0° AoA, and a minimum value at 90°. From this standpoint, the optimum value would be a high AoA during reentry, likely around 90°.

Aerodynamic manoeuver capability for trajectory shaping:
The vehicle needs to manoeuver aerodynamically in the atmosphere by generating lift for several reasons: it allows for trajectory optimization, and it also helps to ensure flight safety thanks to closed-loop trajectory control during reentry. The maximum lift generation occurs with an AoA near 50°, independently from the fins angles. The minimum lift occurs at 0° and 90°. Then, in order to fully modulate the lift, the controllable AoA domain must span from 50° to 90°.
Those constraints are satisfied with a minimum AoA domain between 50° and 90°, which is ensured for a CoM location between -27 m and -30 m. As stated earlier, the heaviest systems (the propulsion systems) will likely be closer to the base than the nose. For this reason, we will now consider the CoM to be still and located at -30 m.

3DoF simulation model and specific aerodynamic control capabilities for a Space X's Starship-like atmospheric reentry vehicle.

5. Lift and drag modulation capacity at a constant equilibrium AoA

5.1. Available control domain for fins angles at iso-equilibrium AoA

Since this vehicle has two sets of actuators, there are several combinations of front and rear fins angles that cancel out aerodynamic moment. Therefore, an equilibrium AoA can be obtained for several combinations of controls. Figure 8 displays the functions $\delta_r = f(\delta_f, AoA_0)$ with the constraint of null aerodynamic moment at the CoM (at Mach 15 and altitude 60 km). It corresponds to a family of all the couples (δ_r, δ_f) that stabilize the aerodynamic moment for a given AoA α_0.

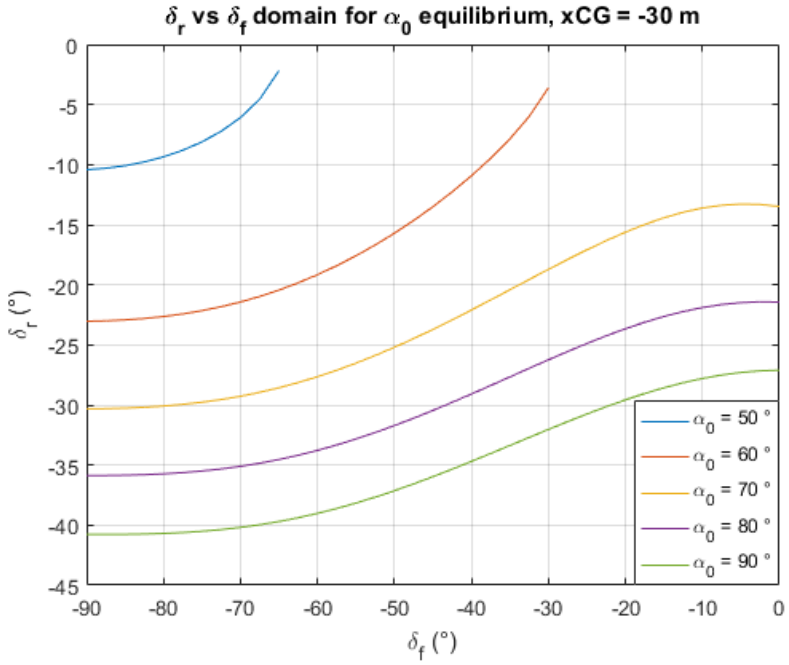

Figure 8 : Front and rear fins angles domain for several equilibrium AoAs

For exemple, at AoA = 90°, the rear fins control angle can vary from -41° to -27° for front fins control angles ranging from -90° to 0°.

5.2. Lift and drag modulation at an equilibrium AoA

Since the fins have a coupled effect on rotational and translational dynamics of the vehicle, the available controls combinations domain at iso-equilibrium AoA allows for modulation of lift and drag without changing the vehicle's attitude. Figure 9 displays the limits of lift and drag acceleration generated by the vehicle at 60 km altitude and Mach 15, versus the desired equilibrium AoA.
As it is visible on these curves, the modulation of drag has greater effects for an AoA near 90°. Concerning lift, the modulation is greater at an AoA close to 65°. The modulation capability is about 12% at best for the lift and drag at their respective preferred AoA. While a 12% modulation does not yield great variations of the aerodynamic forces, it can have a noticeable impact on the final ground distance, as it will be demonstrated on the simulation results presented in the next section.

It is of importance to note that this model does not include friction drag. As a consequence, the results presented here depend on altitude only because of the dynamic pressure in the forces and moment computation. Further work will account for the effect of friction drag on the aerodynamic database and system performance.

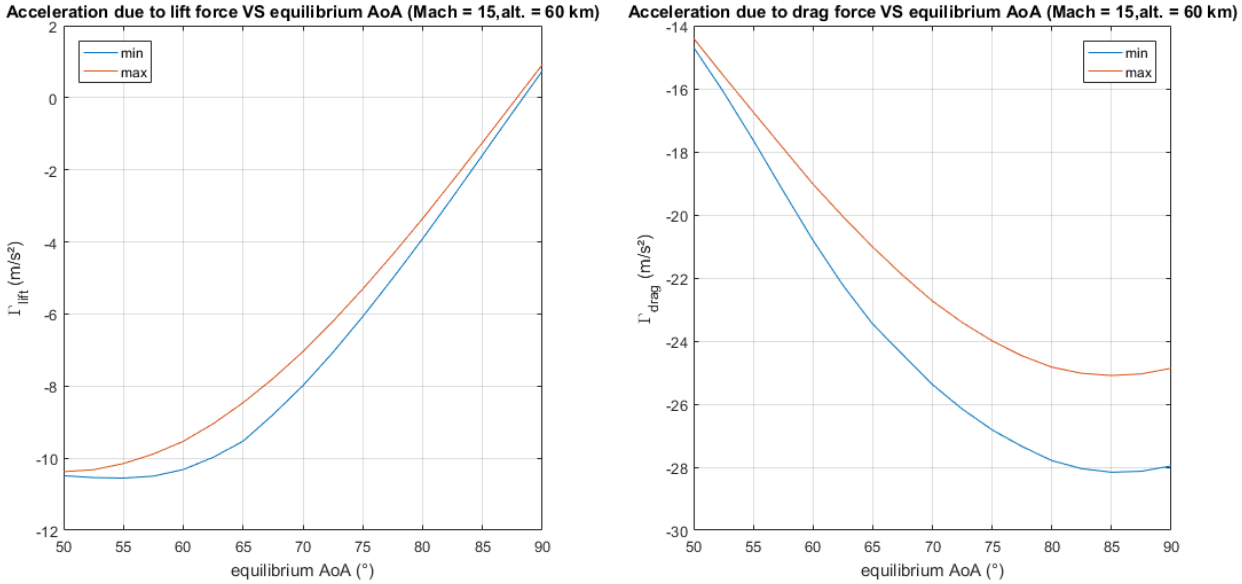

Figure 9 : Limits of lift and drag modulation capability versus stable equilibrium AoA

6. Simulation of translational dynamics

The translational dynamics part of the model has been extracted and used to simulate reentry trajectories of the vehicle in the vertical plan. As it is common for this kind of study, rotational dynamics has been neglected in those simulations for two main reasons: the lack of information about the inertia tensor and pitch damping coefficient Cm_q, and that accurate rotational dynamics simulation often require a much shorter time step than the one use for translational dynamics.
However, the result showed here are still accurate because they can be viewed as simulations of a nominally controlled vehicle in terms of AoA. We use the iso-equilibrium AoA curves of the previous section to select the fins angles to apply depending on the desired AoA. The AoA is considered constant in those simulations.

The reference frame is the local geographic trihedral (North - East – Down, NED). The gravitational acceleration is simply computed as follows:

$$g = \frac{\mu}{(R_T + h)^2} \quad \textbf{(14)}$$

With μ the Earth's standard gravitational parameter (398 600 $km^3.s^{-2}$), R_T the Earth's radius (6 378.139 km), and h the current altitude of the vehicle obtained as follows:

$$h = -z \quad \textbf{(1)}$$

With z the coordinate of the vehicle along the Z axis of the North-East-Down frame.

To account for orbital effects of speed, the vehicle is subject to an apparent gravitational acceleration in the reference frame equal to the summation of g and the centrifugal acceleration. This centrifugal acceleration is computed as follows:

$$Acc_{ctfg} = -\frac{(V.\cos(\gamma))^2}{R_T + h} \quad \textbf{(2)}$$

The atmosphere model used is the US76 model. The Earth is considered still, which means the aerodynamic speed is the same as the inertial speed. Because the aerodynamic characterization method is limited to hypersonic regime, the simulations are interrupted when the vehicle's speed becomes inferior to Mach 4 (the implemented speed limit corresponds to the Mach number reached at 35 km altitude).

3DoF simulation model and specific aerodynamic control capabilities for a Space X's Starship-like atmospheric reentry vehicle.

The state derivatives equations are the following:

$$\begin{pmatrix} \dot{x} \\ \dot{z} \\ \dot{V} \\ \dot{\gamma} \end{pmatrix} = \begin{pmatrix} V.\cos(\gamma) \\ -V.\sin(\gamma) \\ \frac{F_D}{m} - \left(g + Acc_{ctfg}\right).\sin(\gamma) \\ \frac{1}{V}.\left(-\frac{F_L}{m} + \left(g + Acc_{ctfg}\right).\cos(\gamma)\right) \end{pmatrix} \quad \textbf{(3)}$$

With x and z the coordinates of the vehicle in the reference North-East-Down frame, V its speed, γ its flight path angle, m its mass, and F_{Drag} and F_{Lift} respectively the drag force and lift force as explained in paragraph 3.2. The state is initialized with the following values:

Table 2 : Initial state values used in simulation

State parameter	Initial value
x	0 m
z	- 90 000 m
V	7 850 m/s
γ	0 °

6.1. Reentry with different AoAs

To illustrate the diverse aerodynamic capabilities of the vehicle, we computed the trajectories for two constant AoAs during reentry. The first case corresponds to an AoA of 90° (negligible lift), and the second one to an AoA 50° (high lift). The control fins angles have been selected on the curves displayed in Figure 8. Their value is selected on the corresponding AoA curve at the point corresponding to the middle of the δ_f available domain: in the first case we choose $\delta_f = -45°$ and $\delta_r = -36°$, and in the second case we choose $\delta_f = -75°$ and $\delta_r = -8°$. The Figure 10 displays the obtained results for those two simulations.
As it is demonstrated on the *Altitude VS x* plot, the vehicle's ability to fly with an AoA between 90° and 50° will allow for very different reentry trajectories. The load factor is drastically lower on the AoA 50° trajectory (about 1.6 g) than on the AoA 90° trajectory (almost 9 g). It is explained by the fact that aerodynamic lift allows the vehicle to stay longer in the thin high atmosphere which allows it as a consequence to reduce less fast its kinetic energy than in the case without lift. Manned transportation applications and structure design requirements urge to select a reentry trajectory with an AoA allowing for lift generation.

Note that these conclusions heavily rely on initial reentry conditions. With the selected set of initial conditions, in the AoA 50° case, the vehicle generates enough lift force to engage phugoid motion, which is not desirable as we look for a smooth and steady reentry. Simulations with more representative initial conditions will be part of future studies to ensure that phugoid motion still happens with an AoA of 50°. An ideal constant AoA would then be found between 90° and 50° at the lowest AoA without phugoid motion. Future work will also include trajectory optimization using the AoA as time-dependent control parameter.

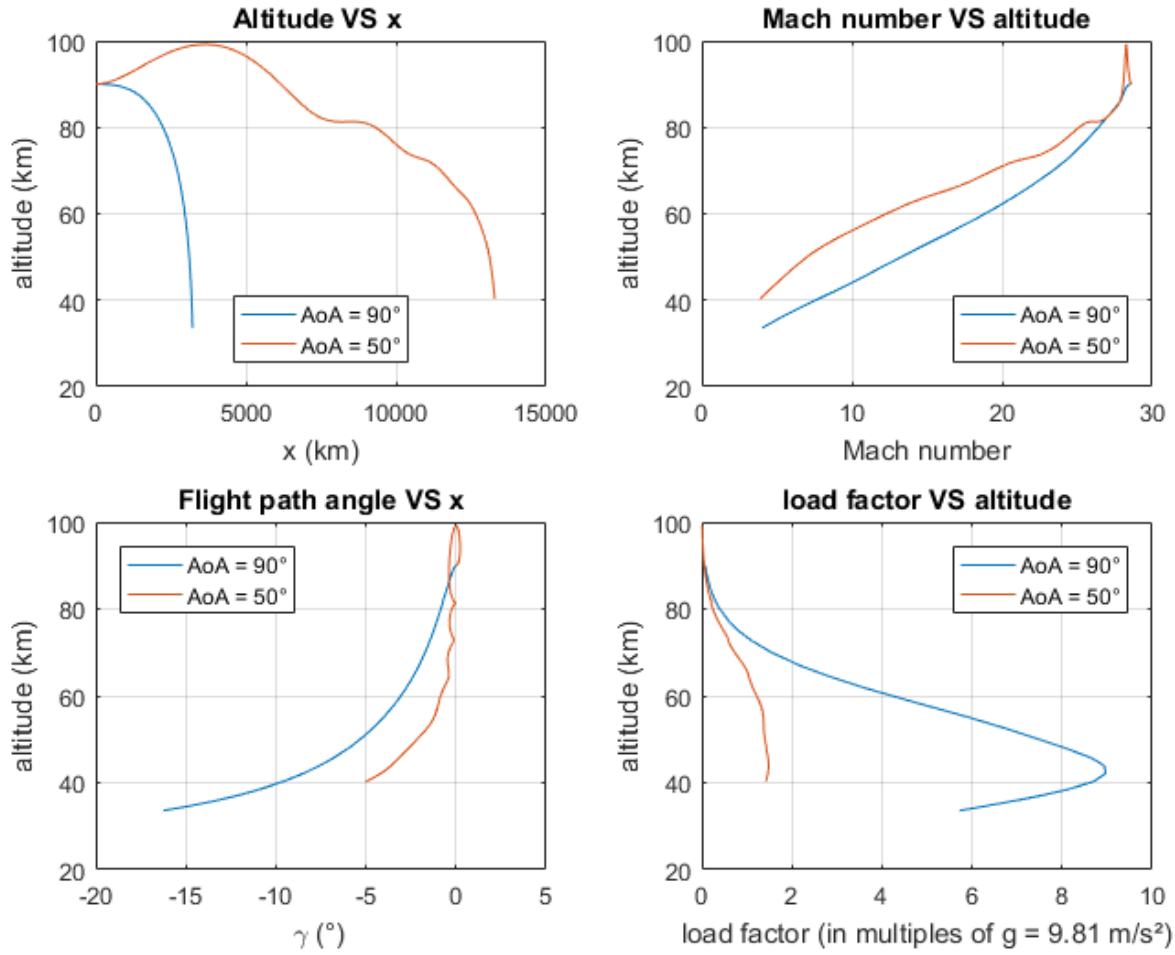

Figure 10 : Illustration of reentries with constant AoAs of 90° (blue curve) and 50° (red curve)

6.2. Reentry at a constant AoA with drag modulation

To illustrate the modulation of aerodynamic force presented in the previous section, we compute the two extreme feasible trajectories for an AoA of 90°. As in the previous paragraph, the control fins angles have been selected on the curves displayed in Figure 8. The first corresponds to fins angles of $\delta_f = -90°$ and $\delta_r = -41°$ (minimum aerodynamic force), and in the second to $\delta_f = 0°$ and $\delta_r = -27°$ (maximum aerodynamic force). Those two control configurations produce sensible difference only in terms of final x distance. The first trajectory stops 120 km further than the second one. Figure 11 displays the trajectory followed by the vehicle in the two scenarios. Further investigation will study why a difference of 12% in aerodynamic forces only implies such little difference in terms of final conditions (about 4% difference on final distance ground distance on figure below).

3DoF simulation model and specific aerodynamic control capabilities for a Space X's Starship-like atmospheric reentry vehicle.

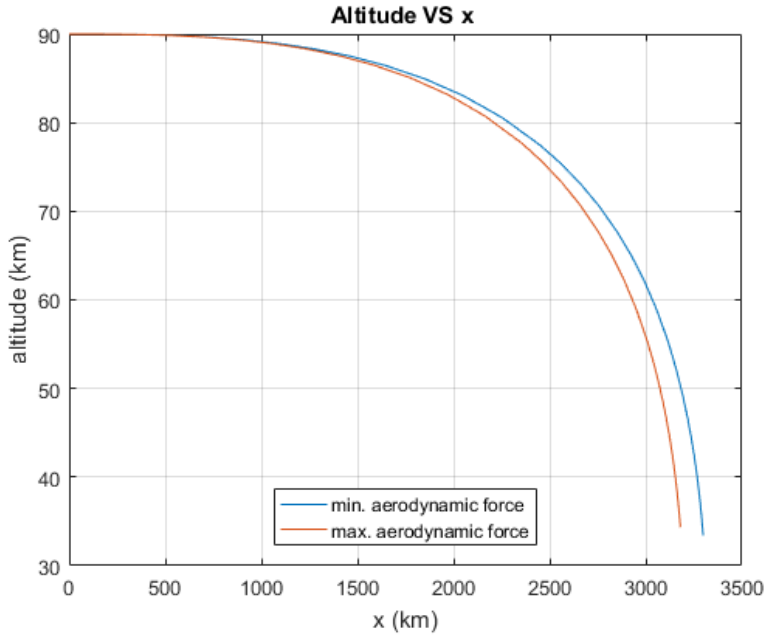

Figure 11 : Illustration of the aerodynamic force modulation capability using two control fins angle configurations for a stable AoA of 90°: $\delta_f = -90°$ and $\delta_r = -41°$ (blue curve), and $\delta_f = 0°$ and $\delta_r = -27°$ (red curve).

7. Conclusion

This study's goal was to render available some data and insights about the aerodynamics of SpaceX's Starship vehicle class. The article presents an estimation of the vehicle's non-viscous aerodynamic coefficients in the hypersonic flow regime dependent on Mach number, angle of attack, and the actuated fins angles. This estimation relies on 3D meshes generated using the OpenVSP tool, and the modified Newtonian theory for local pressure computation. The aerodynamics coefficients reveal little dependence on the Mach number.

An analysis of the longitudinal stability depending on the center of mass' location is also presented. It is shown that this parameter is of great influence on the limits of the AoA domain stabilizable by the actuated fins. As a noticeable conclusion, we observe that a displacement of the center of mass from 30 m to 32 m behind the nose implies a drift of the lower stabilizable AoA boundary from 50° to 80°, which deteriorates drastically the aerodynamic maneuvering capacity of the vehicle.

With the selected set of initial reentry parameters, simulation results at constant AoAs of 90° (non-lifting trajectory) and 50° (lifting trajectory) demonstrates a reduction of the peak load factor from 9 g to 1.6 g. This advocates for lifting reentry trajectories, but will require a more extensive study of reentry trajectories with a more representative set of initial velocity and flight path angle.

On a fixed angle of attack, the multi-actuator configuration (front and rear fins) allowing for aerodynamic force modulation of 12% at best, simulations result demonstrates on the case of study little influence on reentry parameters. We observe a final distance difference of 4% between the two extreme cases.

This preliminary work has arisen numerous questions and needs for improvement of the 3DoF model. Thus, future work will include:

- Reentry simulations with more representative initial conditions ;
- Adding a thermal flux computation model ;
- Trajectory optimization using the AoA as a time-dependent control parameter in order to minimize thermal flux and load factor.

- Estimation of the inertia tensor to allow for rotational dynamics simulation and accurate attitude algorithm design ;
- Creation of a more analytic model fitted on the generated database in order to reduce the computational cost of interpolating the aerodynamic coefficients. Identifying functional dependency of the aerodynamic coefficients to the flight parameters will allow for easier control studies, particularly in the non-linear control field.

8. Acknowledgements

We would like to thank Mathieu Balesdent and Loïc Brevault for their constructive remarks that have enriched this work, and ONERA's Space Programs Direction to provide us the financial means to attend EUCASS 2019.

References

[1] J. R. Gloudemans, P. C. Davis et P. A. Gehlausen, «A rapid geometry modeler for conceptual aircraft,» chez *34th Aerospace Sciences Meeting and Exhibit, AIAA*, 1996.

[2] Space X, «Making Life Multiplanetary,» [En ligne]. Available: https://www.spacex.com/mars.

[3] J. D. J. Anderson, Hypersonic and High Temperature Gas Dynamics, McGraw-Hill Book Company Series in Aeronautical and Aerospace Engineering, 1988.

[4] R. Wuilbercq, Multi-disciplinary Modelling of Future Re-usable Space-Access Vehicles, PhD Thesis, University of Strathclyde, Glasgow, UK, 2015.

[5] L. Lees, «Hypersonic Flow,» chez *5th International Aeronautical Conference*, Los Angeles, CA, 1955.

[6] Space X, «Abridged transcript of Elon Musk's presentation - Making Life Multiplanetary,» 2017. [En ligne]. Available: https://www.spacex.com/sites/spacex/files/making_life_multiplanetary_transcript_2017.pdf.